

Article

Establishing a link between well-ordered Pt(100) surfaces and real systems: How do random superficial defects influence the electrooxidation of glycerol?

Pablo Sebastian Fernandez, Janaina Fernandes Gomes, Camilo Andrea Angelucci, Polina Tereshchuk, Cauê Alves Martins, Giuseppe A Camara, Maria E. Martins, Juarez L. F. Da Silva, and Germano Tremiliosi-Filho

ACS Catal., **Just Accepted Manuscript** • DOI: 10.1021/acscatal.5b00451 • Publication Date (Web): 28 May 2015

Downloaded from <http://pubs.acs.org> on May 31, 2015

Just Accepted

“Just Accepted” manuscripts have been peer-reviewed and accepted for publication. They are posted online prior to technical editing, formatting for publication and author proofing. The American Chemical Society provides “Just Accepted” as a free service to the research community to expedite the dissemination of scientific material as soon as possible after acceptance. “Just Accepted” manuscripts appear in full in PDF format accompanied by an HTML abstract. “Just Accepted” manuscripts have been fully peer reviewed, but should not be considered the official version of record. They are accessible to all readers and citable by the Digital Object Identifier (DOI®). “Just Accepted” is an optional service offered to authors. Therefore, the “Just Accepted” Web site may not include all articles that will be published in the journal. After a manuscript is technically edited and formatted, it will be removed from the “Just Accepted” Web site and published as an ASAP article. Note that technical editing may introduce minor changes to the manuscript text and/or graphics which could affect content, and all legal disclaimers and ethical guidelines that apply to the journal pertain. ACS cannot be held responsible for errors or consequences arising from the use of information contained in these “Just Accepted” manuscripts.

Establishing a link between well-ordered Pt(100) surfaces and real systems: How do random superficial defects influence the electro-oxidation of glycerol?

Pablo S. Fernández^{a,*}, Janaina F. Gomes^{a,†}, Camilo A. Angelucci^b, Polina Tereshchuk^a, Cauê A. Martins^c, Giuseppe A. Camara^d, María E. Martins^e, Juarez L. F. Da Silva^a, Germano Tremiliosi-Filho^a.

^a São Carlos Institute of Chemistry, University of São Paulo, PO Box 780, 13560-970, São Carlos, SP, Brazil.

^b Center of Natural and Human Sciences (CCNH), Federal University of ABC (UFABC), Av. dos Estados, 5001, Santo André, Brazil.

^c Faculty of Exact Sciences and Technology, Federal University of Grande Dourados, 79804-970, Dourados, MS, Brazil.

^d Institute of Chemistry, Universidade Federal de Mato Grosso do Sul, C.P. 549, 79070-900, Campo Grande, MS, Brazil.

^e Physical Chemistry Research Institute (INIFTA), Exact Sciences Faculty, CCT La Plata-CONICET, C.P. 1900, La Plata, Argentina.

ABSTRACT: Glycerol (GIOH) accumulation and its very low price constitute a real problem for the biodiesel industry. To overcome these problems, it is imperative to find new GIOH applications. In this context, electrochemistry arises as an important alternative to the production of energy or fine chemicals using GIOH as a reactant. To make these opportunities a reality, it is fundamentally necessary to understand how the glycerol electro-oxidation reaction (GEOR) occurs on catalysts used in real systems. Thus, research using model surfaces generates the first insight into the electrochemistry of extremely complex real catalysts. Accordingly, in this work, we generate Pt(100) disturbed surfaces in a reproducible manner, carefully controlling the surface defect density. Then, GEOR is studied on well-ordered Pt(100) and on the disturbed Pt(100) surfaces in 0.5 M H₂SO₄ using cyclic voltammetry (CV) and *in-situ* Fourier transform infrared spectroscopy (FTIR). The CV profile of GEOR consists of a single peak in the positive scan. The onset reaction displays the influence of defects present on the surface. On a surface with a high degree of disorder, the main GIOH oxidation process begins at 0.8 V vs. RHE, whereas for well-ordered Pt(100), it starts 0.1 V earlier. FTIR experiments show the presence of carbon monoxide and carbonyl absorption bands. The electrochemical and spectroelectrochemical results are supported by computational calculations (DFT) showing that both CO and GIOH bind more strongly on disturbed than well-ordered surfaces. Thus, our experiments show that Pt-CO (or other GIOH residue) bond breaking may be the GEOR rate determining step.

KEYWORDS: Glycerol Electro-oxidation Reaction, Platinum Single Crystals, Disordered Surfaces, *in situ* FTIR, Density Functional Theory.

INTRODUCTION

Biodiesel has become a real sustainable source of energy to mitigate our dependence to the petro-diesel fuel. However, biodiesel manufacturing leads us to reconsider how environmentally friendly this fuel is given the volume of GIOH resulting from its production: approximately 1 Kg of GIOH per 10 Kg of biodiesel¹. Due partly to the increase in biodiesel production in the last decade, the GIOH supply in the market has outstripped the normal demand (pharmaceutical, cosmetics and food industries), causing a drop in the price of GIOH and consequently problems in distributing the substance excess. Therefore, GIOH has been considered as a potential feedstock for new industrial applications such as the production of more valuable fine chemicals such as dihydroxyacetone, glyceric and hydroxypyruvic acids, 1,2 and 1,3 propanediol, or propylene glycol¹⁻⁵ or direct use as fuel in fuel cells⁶.

However, the main practical difficulty is to selectively produce the desired product from GIOH oxidation, preferably under mild conditions without the use of chromates, permanganates or hypochlorites, which generates industrial waste. In this context, the partial electrochemical oxidation of GIOH on noble metal based-materials seems to be a promising route to overcome this problem.

Accordingly, substantial effort has been devoted to understanding the GEOR and the effect of the variables involved in this process.

Kwon and co-workers⁷ showed that gold catalyzes GIOH oxidation only under alkaline conditions, in contrast to platinum, which catalyzes GIOH oxidation over the entire pH range. In addition to the role of the metal's nature, special attention has been paid to the cation influence on the kinetics of GEOR in alkaline media, showing that non-covalent inter-

1 action between hydrated alkali metal cations and OH_{ad} is present on Pt but absent on Au. Fernandez et al.⁸ studied GEOR using in situ FTIR and isotopically labeled GIOH. The results indicated the presence of CO_2 as a reaction product, implying that GIOH dissociates on Pt surfaces and that C-C bonds can be broken. Studies using Density Functional Theory (DFT) reported that GIOH interacts with the platinum surface via hydroxyl groups,^{9,10} and the interaction of GIOH OH groups with Pt surfaces affects the atomic structure of GIOH compared with the gas phase, in particular, the orientation of the OH groups with respect to the C-C bonds¹¹.

2
3
4
5
6
7
8
9
10
11 In a recent voltammetric study of GEOR on Pt single crystal, it was concluded that the reaction is highly dependent on the surface sites orientation. At low potentials, Pt(111) is more active for GIOH electro-oxidation than Pt(100) and Pt(110)¹²; as seen by in situ FTIR spectroscopy, the reason may be that carbon monoxide, a common adsorbed intermediate of organic molecules oxidation on Pt, was more easily removed from Pt(111) than from Pt(100) and Pt(110).¹³ These results of GEOR performed on well-ordered surfaces follow the trend of structure sensitivity of most electrochemical reactions, namely: hydrogen¹⁴, carbon monoxide¹⁵, methanol¹⁶, ethanol¹⁷, ethylene glycol^{18,19} oxidation, oxygen²⁰ and nitrate^{21,22} reduction, among others.

12
13
14
15
16
17
18
19
20
21
22
23 In this way, the relationship between the different site symmetries at the electrode surface and its electroactivity response provides a powerful tool for designing nanocatalysts for practical uses²³⁻²⁵. Therefore, the use of well-ordered surfaces to understand the key role played by the surface structure underwent great improvement after the publication of the “flame annealing method” by Clavillier et al.²⁶. The presence of dilute defects on single crystal surfaces, known as stepped surfaces, allows the systematic study of the influence of well-defined defects in different systems. The usual approach is to begin with a very well-ordered surface, without defects, and proceed toward more complex systems using stepped surfaces with different quantities of a given defect (steps or kinks at different surface geometries), providing the decrease of terrace domains in detriment of defects.

24
25
26
27
28
29
30
31
32
33
34
35
36
37
38
39
40
41
42
43
44
45
46
47
48 Despite these advances and some insights published in our previous work¹², it remains unclear how the role of surface defects influences the GEOR. For this investigation, we electrochemically generate a set of Pt(100) surfaces with a controlled density of defects and with diverse defect symmetry. This strategy presents a new path to linking well-ordered with disordered surfaces, using a set of surfaces with non-defined defects (in contrast to the well-defined defect of the stepped surfaces). It is a highly reproducible method and could be potentially applied in other systems, not necessarily in electrochemistry.

49
50
51
52
53
54
55
56
57
58
59
60
61 Then, with the aim of understanding the GEOR mechanisms on platinum at different degrees of surface order, moving from an ideally ordered to highly disordered surface and hence approaching the highly disordered real systems, we used the electrochemically generated disturbed surfaces to study the GEOR. Conventional techniques such as CV and FTIR were combined with DFT. The results showed that the disturbed surfaces are poorer catalysts than the well-ordered Pt(100) single crystal and appear to be connected with the stronger Pt-CO bonding on the low-coordinated Pt atoms of disturbed surfaces.

EXPERIMENTAL SECTION

Electrochemical systems and spectroelectrochemical experiments.

All of the experiments were performed at room temperature ($25 \pm 1^\circ\text{C}$) in a conventional three-electrode electrochemical cell. A high-area polycrystalline Pt sheet was used as a counter electrode. The reference electrode was a reversible hydrogen electrode (RHE). The working electrode was a 1-cm diameter Pt(100) disc acquired from MaTeck.

In order to check the platinum surface order, cyclic voltammograms (CVg) were obtained in the potential range between 0.05 V and 0.80 V in a 0.5 M H_2SO_4 solution. The solution cleanliness was checked by the stability of the voltammetric features of Pt electrodes. The upper potential limit was set to avoid any Pt oxide formation, which generates irreversible surface disordering.

The FTIR instrument was a Nicolet Nexus 670 spectrometer equipped with a liquid nitrogen-cooled MCT detector. In situ FTIR experiments were performed in a three-electrode spectro-electrochemical cell with a planar CaF_2 window attached to the bottom of the cell. Details concerning the cell are described elsewhere²⁷. Briefly, a movable piston supports the working electrode. A Pt wire connected to the working electrode passes through the piston and maintains the electrical contact. The CaF_2 window functions as a transparent cell bottom and as a wall against the working electrode. It is pressed to obtain a thin film of electrolytic solution. In this way, the absorption of the infrared beam by the solution is minimized during the FTIR measurements.

The FTIR spectra were computed from an average of 128 interferograms. The spectral resolution was set to 4 cm^{-1} . First, the working electrode was placed in the meniscus configuration, and five consecutive CVg were obtained in a solution of 0.2 M GIOH and 0.5 M of H_2SO_4 . The potential was kept at 0.12 V, and the electrode was dipped in the solution until it contacted the window. When the system became stable (the recorded spectra did not change with time at 0.12 V and were set as reference spectra) a linear potentiodynamic sweep was started at 0.002 Vs^{-1} , and the scan was stopped every 0.005 V for enough time to obtain 128 interferograms (approximately 1 minute). Thus, the first spectrum was obtained at 0.15 V, the next at 0.20 V, and so on until 0.95 V. The choice of this upper potential limit will be explained below.

Working electrode surface preparation.

To obtain perfectly ordered and clean surfaces, the working electrode was flame annealed in a butane-oxygen flame for one minute and cooled in a reductive $\text{H}_2 + \text{Ar}$ atmosphere for five minutes. The electrode surface was then protected with a water droplet saturated with cooling gases to prevent contamination and reconstruction of the surfaces during the transfer to the electrochemical cell.

To monitor the influence of the upper potential limit on the Pt(100) surface order degree, the potential limit was progressively augmented from 0.80 V until 1.05 V. Through this experiment, we determined that: i) the Pt(100) surface cycled until 0.95 V remains unchanged and very well ordered (at least for some cycles) and ii) cycling up to 1.05 V progressively generates more and more disordered Pt(100) surfaces. This limit is low enough to permit surface order monitoring (through some characteristic voltammetric features that are

discussed later) and thus gives the possibility of stopping the experiments after obtaining a surface with the desired defect density. The incursion in higher potentials (above 1.05 V) can cause severe surface disordering even in the first cycle²⁸. After this experiment, the upper potential limit was set to 0.80 V again to obtain a CVg of the modified Pt(100) surface (blank CVg) for direct comparison with the very well-ordered Pt(100) surface.

In this work, five different disordered Pt(100) electrodes were obtained. In ascending order of defect density, they are as follows (the different electrode names PtX-Y will be explained later): i) Pt0-100 = Perfectly ordered surface; ii) Pt25-75 = Surface obtained after 4 CVg up to 1.05 V; iii) Pt50-50 = Surface obtained after 8 CVg up to 1.05 V; iv) Pt75-25 = Surface obtained after 16 CVg up to 1.05 V; v) Pt100-0 = Surface obtained after 25 CVg up to 1.05 V + 12 CVg up to 1.20 V. In this last case, the potential limit was changed to obtain a completely disordered Pt(100) surface.

Once the desired surface was prepared, the platinum surface order was checked again performing CVg in the potential range between 0.05 V and 0.80 V in a 0.5 M H₂SO₄ solution. Then, it was protected with an electrochemical solution droplet and transferred to another identical electrochemical cell containing a 0.5 M H₂SO₄ and 0.2 M GIOH solution. The Pt(100) surface was placed in contact with the solution at 0.12 V in all experiments. This potential was chosen to minimize faradaic processes other than GIOH dissociative adsorption²⁹.

Theoretical approach and Computational details.

We investigated the structural and energetic properties of GIOH and carbon monoxide (CO) on the Pt(100) surface using DFT within the generalized gradient approximation proposed by Perdew-Burke-Ernzerhof (PBE)³⁰ for the exchange-correlation (xc) energy functional. To solve the Kohn-Sham equations, we employed the Vienna Ab-initio Simulation Package (VASP)^{31,32} with the all-electron projected augmented wave (PAW) method implemented^{33,34} and the PAW projectors to describe the electron-ion interactions. For all of the total energy surface calculations, a plane-wave cutoff energy of 487 eV was used, whereas for the integration of the Brillouin zone (BZ), a 3×3×1 kpoint mesh was used. We obtained the equilibrium atomic positions once the atomic forces on each atom were smaller than 0.025 eV/Å with a total energy convergence of 10⁻⁵ eV.

The unreconstructed Pt(100) surface was obtained using a periodic surface slab model of six layers' thickness with a (4×4) surface unit cell (16 Pt atoms per plane) and a 20 Å vacuum region. The defected Pt(100) surface was modeled based on the unreconstructed Pt(100) surface model where 10 surface atoms were removed and the remaining 6 atoms on the surface have lower coordination; thus, this surface has less coordinated sites and terraces (this surface will be termed Pt₆/Pt(100) in our discussion to differentiate it from the electrochemically prepared disordered surfaces). The molecules adsorbed only on one side of the slab. Only the bottom layer of the slab was frozen, while the other five layers along with the adsorbates were allowed to relax in all calculations.

To study the complicated structure of the CO-GIOH mixture on the disordered Pt(100) surface, i.e., Pt₆/Pt(100), we searched for the lowest energy configurations by performing

the following steps. (i) Several initial configurations were presented with three CO molecules initially adsorbed at the different positions on the unreconstructed Pt(100) surface, i.e., top, bridge and hollow sites and their combinations, to identify the correct adsorption site on the clean Pt(100) surface. All of the configurations were optimized using the standard optimization procedure of VASP, in which the lowest energy configuration with the right adsorption site was selected and used in the next steps of the simulation. (ii) We then modeled the configurations in which CO molecules were located on the lower and higher coordinated sites of the Pt₆/Pt(100) surface, i.e., terraces and islands, and their combination, (iii) We simulated GIOH adsorption on our surfaces. It is important to note that in our previous work, we carefully investigated GIOH configurations on Pt(hkl) surfaces using ab initio molecular dynamics simulation and found the lowest energy configuration for GIOH on Pt(100)¹¹. We revealed that GIOH binds with the Pt(100) surface with the adsorption energy of -0.44 eV via the O atom, where the distance between the O and Pt atom is 2.45 Å, and the angle between the bonds of the edge C atoms and the surface normal is 79.46°. In this work, employing the GIOH structure on the previously obtained clean Pt(100) surface¹¹, we modeled different atomic configurations of GIOH on the Pt₆/Pt(100) surface, where GIOH adsorbed on the lower coordinated sites and on the terraces. (iv) Complex systems consisting of three CO molecules and GIOH on the Pt₆/Pt(100) surface were simulated using the lowest energy structure of GIOH on the Pt₆/Pt(100) surface, in which CO molecules were bound on different positions of the surface, i.e., the lower coordinated sites and the terraces. All structures were optimized employing the standard VASP optimization procedure.

To analyze the lowest energy structures, we computed adsorption energies by applying the following formulas: $E_{ad} = E^{tot-system} - (3 * E^{CO} + E^{clean Pt})$ for 3 CO, $E_{ad} = E^{tot-system} - (E^{GIOH} + E^{clean Pt})$ for GIOH and, $E_{ad} = E^{tot-system} - (3 * E^{CO} + E^{GIOH} + E^{clean Pt})$ for the GIOH and 3CO mixture on Pt surface. Here, $E^{tot-system}$, E^{CO} , E^{GIOH} , and $E^{clean Pt}$ are the total energies of the system, CO and GIOH molecules in gas-phase, and the clean Pt surface, respectively.

RESULTS AND DISCUSSIONS

Pt(100) modified electrodes.

TEM and STM are typical ex-situ characterization techniques. The former is very useful for identifying the size and shape of nanomaterials, whereas STM could provide valuable information on our surfaces. However, these techniques are time consuming and expensive, and they provide only local information. Sometimes, even by taking images of an important quantity of different surface regions, it is impossible to extrapolate the results to the whole electrode surface. In this context, surface characterization techniques in the metal-solution interface are well-established as the best tool to monitor the different symmetry sites in this type of system, providing us an overall response of the surface in contact with the electrochemical solution. Thus, the so-called hydrogen adsorption/desorption region is very useful for qualitative characterization of the Pt surfaces^{23,28,35-37}. In this way, the CV profile for the platinum electrode is considered a fingerprint of the surface structure, giving us information about the symmetry and distribution of the surface sites, as well as the system's general conditions and cleanliness. Therefore, our starting

point in this work was to analyze the electrode surface structure from the density current response displayed in the CVg recorded in only the sulfuric acid electrolyte.

Figure 1 (black line) shows the blank CVg of a well-ordered Pt(100) electrode. The profile presented is consistent with other published results, characterized by a narrow peak at 0.37 V with a symmetrical density current in the positive and negative scan³⁸. Any surface structure modification leads to a change in the CV profile. Specifically for Pt(100) electrodes, changes can be easily identified by (i) decreases in the characteristic peak at 0.37 V, (ii) the appearance of a peak at 0.26 V - 0.28 V and (iii) increases in the density current below 0.20 V, as seen in Figure 1A for the Pt25-75, Pt50-50, Pt75-25 and Pt100-0 electrodes. The current signals at 0.26 V - 0.28 V and below 0.20 V were previously assigned to hydrogen adsorption/desorption on border or step sites with the (110) and (111) orientations, respectively^{35,38,39}.

The terminology PtX-Y refers to the intensity of the peak at 0.26 - 0.28 V (X) and of the peak at 0.37 V (Y). Pt0-100 stands for the perfectly ordered Pt(100) surface. The corresponding CVg presents only the peak at 0.37 V (Y). Consequently, for Pt0-100, X=0 and Y=100. Pt50-50 represents the surface presenting features at 0.26 - 0.28 V (X) and 0.37 V (Y) with approximately the same intensity. Pt100-0 represents the totally disordered Pt(100) surface, for which the corresponding CVg presents only the peak at 0.26-28 V. Pt25-75 and Pt75-25 are electrodes presenting less and more defective surfaces than Pt50-50, respectively.

To achieve systematically different surface electrode configurations and study the influence on GIOH oxidation, we applied successive cycles on the Pt0-100 electrode up to 1.05 V, keeping the lower potential at 0.05 V. Figure 1B shows the surface modification during 25 consecutive CVg. This 25 CVg are only applied to obtain the Pt100-0 surface. When a more ordered surface is desired, for instance, the Pt50-50, the cycling until 1.05 V is stopped after the 4th cycle and the blank CVg is recorded again. Thus, the electrochemical features of the disturbed electrodes (blank CVg) after the surface modification procedure are displayed in Figure 1A. (Figure S1 shows the complete cycling for the generation of Pt100-0).

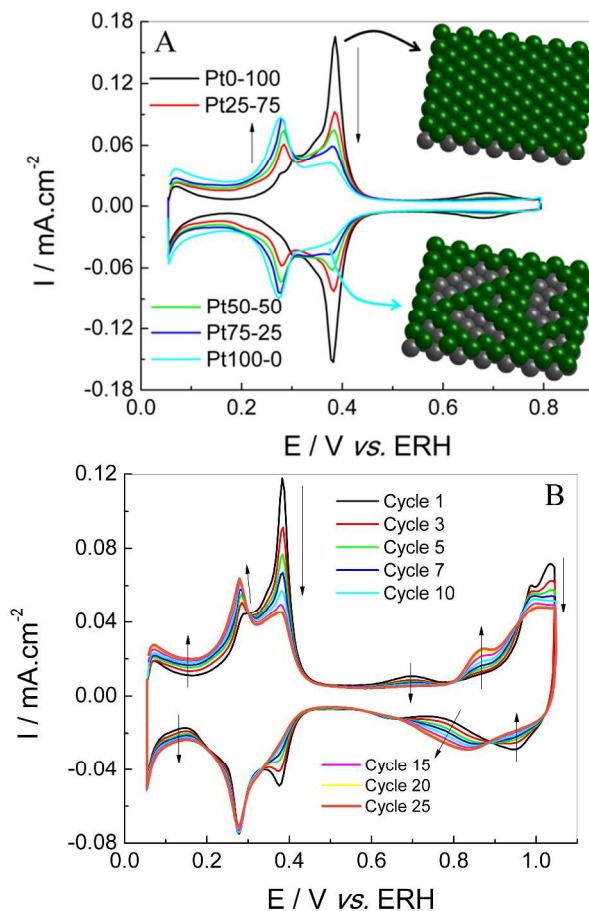


Figure 1. (A) Voltammograms obtained in 0.5 M H₂SO₄ solution for the different defect density Pt(100) surfaces. The black CVg shows the typical electrochemical features of an ordered Pt(100) surface, and the light blue CVg corresponds to a highly and randomly disordered surface. (B) Generation of disordered electrode by cycling up to 1.05 V. $\nu = 0.05 \text{ Vs}^{-1}$.

It is well known that the excursion into the oxygen adsorption region causes intense surface structural modification⁴⁰. In Figure 1B, the evolution of the continuous cycling is characterized by changes in the hydrogen adsorption/desorption region ($E < 0.4 \text{ V}$) and the appearance of a redox response at potentials above 0.80 V. The formation of a submonolayer oxide film, recognized as OH and O electroadsorption⁴¹, leads to a progressive and irreversible transformation of a well-defined 2-D surface to one in which the local order is continuously changed by covering the surface with defects. Such defects can be assigned as single ad-atoms, small islands, pits or other collections of defects, as described by Björling and Felin⁴² for a series of experiments in the study of oxide formation on Pt stepped surfaces. In addition to the changes in the hydrogen adsorption region, the appearance of defects sites/domains on the surface leads to hysteresis in the current response during the anodic oxygen adsorption and cathodic reduction of the oxide film.

The CVg of the electrochemically disordered Pt100-0 electrode indicates that the surface retains the symmetry of the (100) sites, but with a depletion of the large domains with the increase of the cycles into the oxygen adsorption region. The quantification of the actual (100) terrace sites at every modified electrode is not a simple assignment determined solely by

the analysis of the blank CVg. Solla-Gullón et al.⁴³ proposed a quantitative method for the estimation of surface sites on Pt samples using specific site-probe reactions. However, in this work, we achieved the presence of the (100) domains and the surface defects' influence on GEOR without a quantitative estimation of the specific surface orientation. On the other hand, the "soft" damage caused by cycling into the early stages of oxygen adsorption potentials showed that we can produce a surface with a systematic decrease of large terrace domains.

At this point in the work, it is interesting to clarify the differences in surface structures presented in a model single crystal electrode produced with systematic density defects (stepped surfaces) and the ones produced in this work. Although the CV profiles of Pt stepped surfaces are highly similar to the ones displayed here, the assignment of the specific kind of defect (kinks and steps), as well as the terrace width distribution, on Pt(100) modified electrodes is not straightforward without their characterization by additional techniques^{42,44} and experiments.

GLOH electrooxidation on Pt(100) surfaces.

Figures 2A and 2B show five consecutive CVg for Pt0-100 and Pt100-0, respectively. The CV features for GEOR change progressively from the well-ordered surface, Pt0-100, to the totally disturbed one, Pt100-0. Thus, for the sake of clarity, we decided to present the two limit behaviors (Figure S2 shows the Pt50-50 behavior).

In general, the first CVg for GEOR on Pt0-100 and Pt100-0 presents current signals at 0.20 V - 0.70 V and a sharp oxidation peak close to 0.80 V - 0.85 V in the positive-going potential scan and a reactivation wave between 0.95 V and 0.4 V in the negative-going potential scan. Remarkably, as the density of defects increases, the sharp oxidation peak in the positive scan becomes thinner. The current signals at 0.20 V - 0.70 V vanish from the first to the second CVg for both electrodes. From the second to the fifth CVg, the changes are not significant, especially for Pt0-100. After the fifth potential cycle, the changes in the CV profile for both electrodes become negligible.

As mentioned above, the main difference between the first and the subsequent CVg is the presence of current signals between 0.20 V and 0.70 V, which are present only at the first potential cycle. These current signals are related (at least in part) to GIOH and hydrogen/anion co-adsorption, as seen in the insets in Figures 2A and 2B, and the lack of them from the second potential cycle on demonstrates that the adsorption layer formed at 0.12 V when the electrode is put in contact with the solution is clearly distinct from the adsorption layer formed at the beginning of the second CVg after the excursion to higher potentials. In particular, the absence of any current signal between 0.20 V and 0.70 V indicates that the surfaces are completely blocked by the adsorption of GIOH or its derivatives in this potential region.

Detailed analysis of the first CVg (Figures 2A and B) reveals important differences between the GEOR on Pt0-100 and Pt100-0. In the positive-going potential scan, while the perfectly ordered surface shows a small peak in the co-adsorption region and a pre-wave before the main oxidation peak, the totally disturbed surface presents important oxidation peaks from 0.2 V to 0.95 V. Therefore, the defects favor the oxidation of the GIOH residues at low potentials in the first positive-going potential scan. Interestingly, in the next scans,

when the surfaces are completely blocked at lower potentials, the defects act in a contrary manner, increasing the potential needed to oxidize the GIOH molecules and/or their derivatives, as seen by the potential of the sharp peak, which is higher for Pt100-0 than for Pt0-100. These results show that the defects strongly influence the surface responses in the positive-going potential scan.

In addition, in the negative-going potential scan, the CV profile of the reactivation wave also depends on the density of the surface defects. For Pt100-0, this signal shows at least two different contributions. The first peak is centered at approximately 0.70 V and the second one at approximately 0.50 V. The peak at 0.70 V coincides with the one for Pt0-100. This result suggests that this contribution is connected to extended well-ordered surfaces and the one located at lower potentials appears to be connected with the reactivation of the disordered domains.

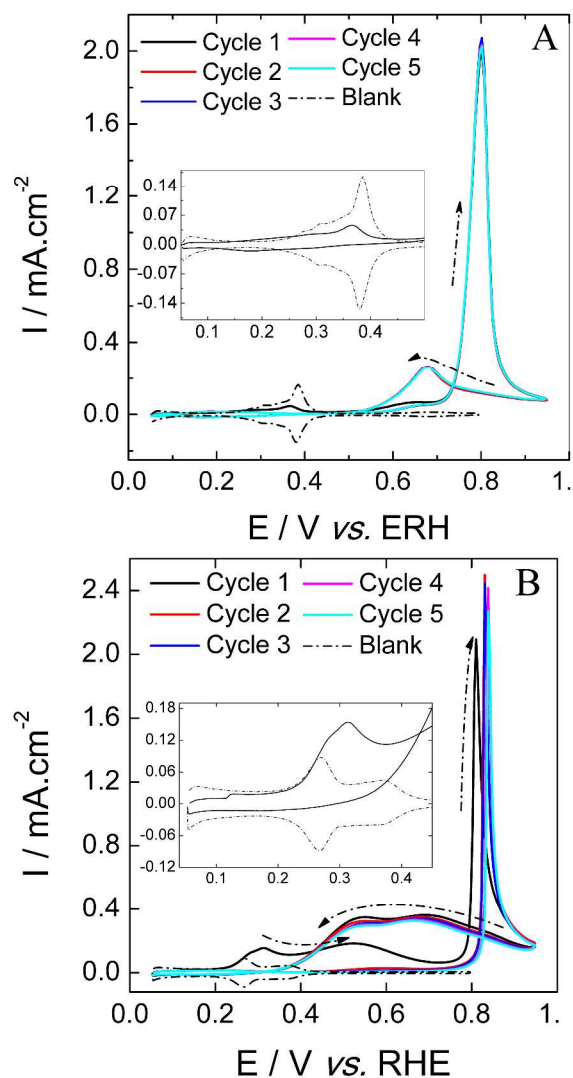


Figure 2. CVg obtained in 0.2 M GIOH and 0.5 M H₂SO₄ solution with Pt0-100 (A) and Pt100-0 (B). $v = 0.05 \text{ V s}^{-1}$.

To further evaluate the impact of the surface defects on GEOR over modified Pt(100), the onset potential and the potential of the sharp peak were extracted from the fifth positive-going potential scans (shown in Figure 2A and B) and plotted as a function of the density of surface defects. These

data are presented in Figures 3A and 3B. Figure S3 shows the process used to calculate the onset potential for every electrode.

Figure 3A shows a continuous displacement of the onset potential towards more positive potentials with increasing density of surface defects. In particular, from the perfectly ordered surface to the totally disordered one, the onset potential shifts by approximately 100 mV (Figure 3A), which is a significant change in terms of energy. The potential of the sharp peak follows the same trend as a function of the density of surface defects (Figure 3B), although it is less sensitive to the presence of defective sites than the onset potential. Therefore, these results clearly demonstrate that in steady-state conditions (at the fifth CVg), as the density of surface defects increases, more energy is necessary to oxidize GIOH and its derivatives.

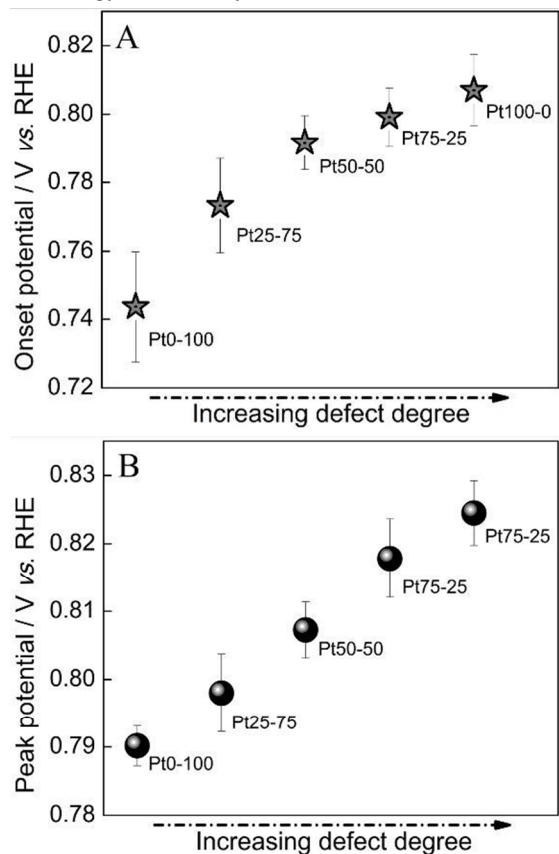


Figure 3. Changes in the onset potential (A) and in peak potential (B) of the GEOR as a function of the degree of electrode defects.

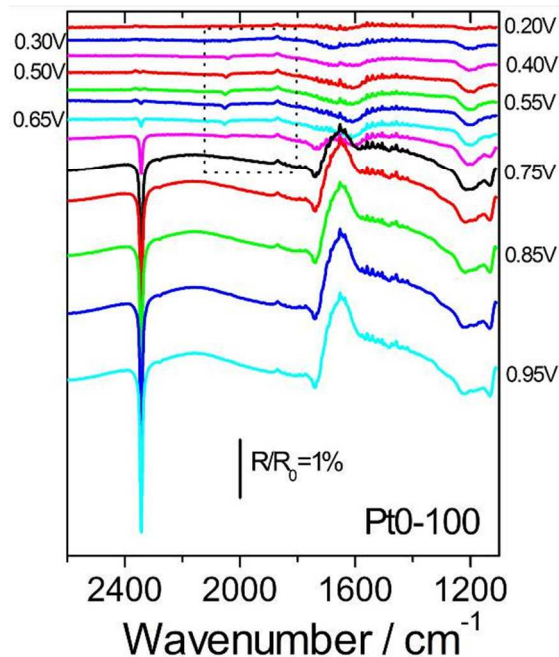
Returning to Figure 1B, we see that the continuous defect generation produces a displacement of the oxide formation domain to lower potentials. It is generally accepted that the onset potential of the oxidation of small organic molecules is connected to the Pt-OH formation. Thus, the Pt-OH species react with the pre-adsorbed molecules (generally through a Langmuir-Hinshelwood mechanism), producing several products and thus generating positive currents. As we previously showed, our results are not consistent with this idea, as we observed an increase in onset potential for electrodes that form Pt-OH at lower potentials. Clearly, this description is an oversimplification of a very complicated system, where water, anions, cations and organic molecules compete at different potentials, sometimes for a myriad of diverse Pt adsorption

sites (where diverse adsorption sites imply different sites configurations and adsorption energies).

FTIR *in situ* experiments.

Figure 4 shows some selected spectra obtained with Pt0-100 and Pt100-0. In Table S1, the main band assignments can be observed. A band centered at 2343 cm^{-1} corresponding to the asymmetric stretching of CO_2 is present for both surfaces. Additionally, a band centered at 2040 cm^{-1} , whose frequency varies with the working electrode (frequency variation is shown in Figure S4), is attributed to the on-top bonded CO and is also present for both surfaces. Another very important feature at approximately 1740 cm^{-1} corresponding to carbonyl containing compounds ($\text{C}=\text{O}$) can be observed in Figure 4, and a detailed inspection of this band shows that it consists of at least two superimposed signals (see Figure S5). Again, this signal is also present for both surfaces. Lastly, at least three bands between $1100\text{--}1300\text{ cm}^{-1}$ can be observed. Briefly, they correspond to the generation of carboxylic acids, the consumption of GIOH and the entrance of SO_4^{2-} and HSO_4^{-} ions in the thin layer during the potential scan. Unfortunately, the signal of the anions (both in the solution and bound to Pt) is too strong to permit a clear observation of other interesting signals present in the same wavenumber domain. The same general features were previously observed by Gomes et al.¹³

Figure 5 reveals details of the bands in the wavenumber region between 2100 cm^{-1} and 1800 cm^{-1} . For Pt0-100, a positive band located at approximately 1870 cm^{-1} corresponding to bridge-bonded CO is seen from 0.30 V on. In contrast, for Pt100-0 a negative band at approximately 1840 cm^{-1} with a very low intensity also corresponding to bridge-bonded CO can be seen. These results clearly indicate that bridge-bonded CO was already present at the beginning of the experiment at 0.12 V for Pt0-100 but not for Pt100-0.



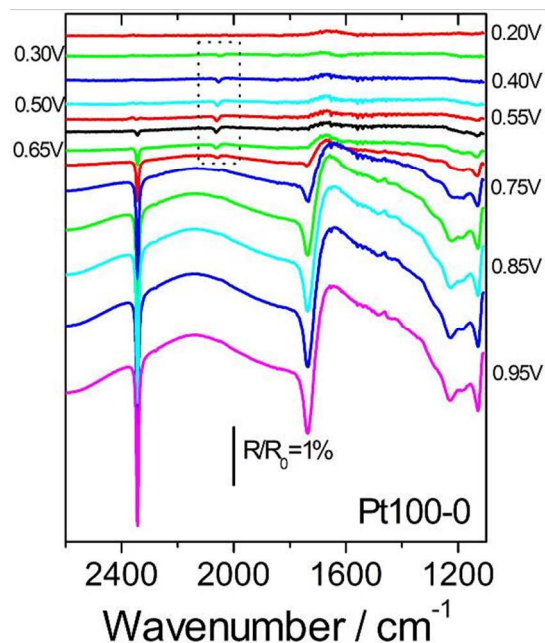


Figure 4. Selected FTIR spectra obtained at different working electrode potentials in 0.2 M GIOH + 0.5 M H₂SO₄. Spectra obtained at lower potentials do not show any important difference with respect to the background spectra obtained at 0.12 V.

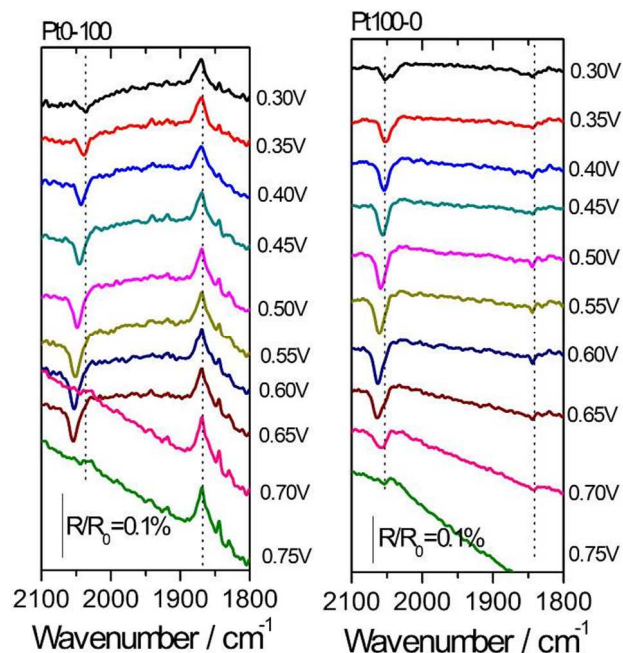


Figure 5. This picture shows an enlarged view of the rectangular region of Figure 4 drawn with dashed lines. Both surfaces show signals attributed to on-top and bridge-bonded CO.

The behavior of the bands corresponding to on-top bonded CO, CO₂ and C=O formation (shown in Figure 4) as a function of the electrode potential is further evaluated in Figure 6. To construct this figure, CO and CO₂ bands were integrated along the potentiodynamic sweep. As the C=O band superimposes with a broad positive band at 1630 cm⁻¹ due to the continuous exit of water from the thin layer, the C=O band area is not clearly defined and for this reason could not be integrated. To quantify the production of C=O containing compounds, we

measured the variations in peak intensity with respect to a baseline passing through the left queue of the C=O band, at the opposite side of the water band (Figure S6).

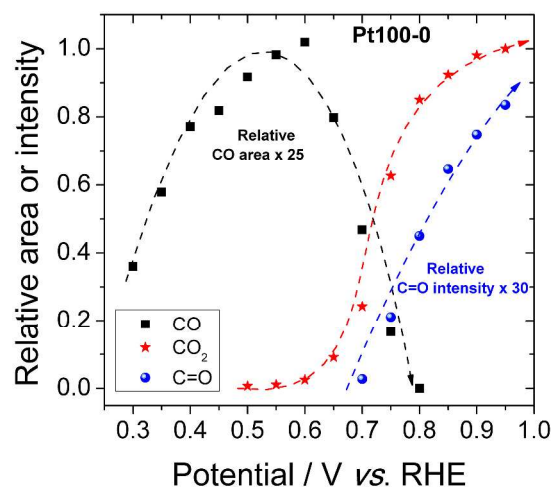
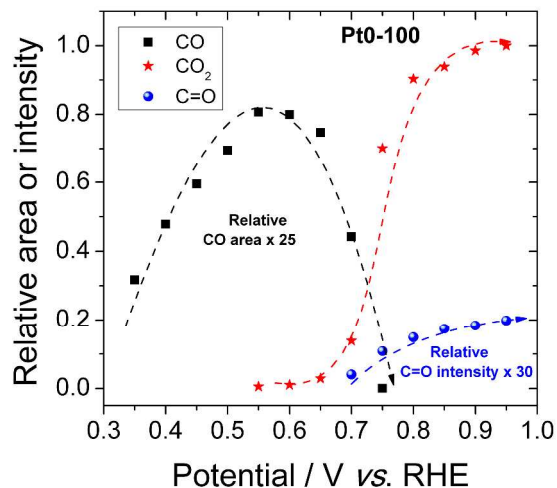


Figure 6. Intensities of C=O and absorbances of on-top bonded CO and CO₂. Both intensities and absorbances were divided by the corresponding maximum CO₂ band absorbance, i.e., the CO₂ band integration value obtained at 0.95 V. Figure S7 shows the crude results for two independent measurements.

As seen in Figure 6, CO is formed on Pt0-100 and Pt100-0 at low potentials (the first discernible signal appears at 0.30 V), and its production increases continuously until attaining a maximum at approximately 0.60 V, when it suddenly decreases. This abrupt decrease occurs in the same potential domain where the CO₂ formation increases quickly. It is reasoned to be a consequence of the oxidation of GIOH to CO₂, with CO as a reaction intermediate. Interestingly, the amount of on-top bonded CO with respect to CO₂ is fairly different for Pt0-100 and Pt100-0, being higher for the disordered surface, suggesting that Pt100-0 exhibits greater ability in C-C bond breaking and converting CO into CO₂. On the other hand, for Pt0-100, CO₂ may be formed in part through a pathway that does not involve CO as an intermediate. The behavior of the on-top bonded CO and CO₂ formation is very similar to the behavior found by our group in previous works⁸. The development of these species on the Pt100-0 surface is shown in this work for the first time.

A very interesting result is that C=O formation was observed from 0.70 V on both surfaces, that is, 0.10 V after beginning

1 the CO oxidation. This result suggests that GIOH and CO
2 compete for catalytic sites, with CO being the main adsorbate
3 at low potentials, whereas GIOH can massively adsorb at
4 relatively high potentials to produce CO₂ through a direct
5 pathway or be oxidized to form C=O with or without C-C
6 bond breaking (the main C=O signals observed for polycrystalline Pt in the same potential domain used in this work come from glyceraldehyde and glyceric acid⁷).

8 By comparing the ratio between C=O and CO₂ produced on
9 Pt(100) and Pt(100)-0, a very important observation arises from
10 both the basic and applied perspectives. On the disturbed
11 surface, the formation of carbonyl containing compounds
12 increases rapidly and continuously along the potential scan,
13 whereas on the well-ordered surface, the signal changes only
14 slightly between 0.80 - 0.95 V. To exemplify, at 0.95 V, the
15 ratio between C=O and CO₂ formed on the disturbed surface is
16 approximately 6 times higher than on the well-ordered surface.
17 This difference is important and might be useful from a tech-
18 nological perspective. This type of experiment may serve as a
19 starting point for the selective production of C=O GIOH der-
20 ivatives, assisting in the choice of an appropriate real catalyst
21 (e.g., nanomaterials) with a suitable shape for the production
22 of GIOH derivatives with added value^{45,46}.

23 Density Functional Theory Calculations.

24 To gain further insight on GEOR, we performed computa-
25 tional calculations including modeled well-ordered and disor-
26 dered Pt(100) surfaces. In addition, the stability of these sys-
27 tems in the presence of CO, GIOH and CO+GIOH was care-
28 fully studied.

29 *Structural and adsorption properties.* The lowest energy con-
30 figurations for 3CO, GIOH and the 3CO+GIOH mixture on the
31 Pt(100) and Pt₆/Pt(100) surfaces are shown on Figure 7. High-
32 energy isomers are shown in the supporting information (S8-
33 S11). We found that CO molecules bind to the Pt(100) surface
34 via C atoms on the bridge sites and that moving one of the CO
35 molecules to the top site of Pt(100) increases the total energy
36 of the system by 0.25 eV (Figure S8). On the Pt₆/Pt(100) sur-
37 face, we observed that all of the CO molecules prefer binding
38 on the low coordinated Pt₆ atoms (Figure 7). We expected
39 from the CO/Pt(100) calculations that all of the CO molecules
40 would be located on the bridge sites; however, we found that
41 only 2 molecules are located on the bridge sites of the low
42 coordinated Pt₆ atoms, whereas one CO adsorbs on-top of the
43 edge low coordinated Pt₆ atom due to the release of the strain
44 from the molecular repulsion. The configuration in which all
45 CO molecules bind on bridge sites of Pt₆ is only 0.16 eV high-
46 er in energy than the lower energy configuration, which means
47 that this configuration might exist under certain experimental
48 conditions, e.g., in high-temperature experiments. Surprisingly,
49 the adsorption of CO is slightly stronger on Pt(100) than on
50 the Pt₆/Pt(100) surface (by 0.07 eV), considering the presence
51 of the low coordinated atoms on the Pt₆/Pt(100). The given
52 quantity of CO molecules (i.e. three molecules) was chosen by
53 us for our DFT calculations in order to take into account the
54 intermolecular interaction and binding of CO molecules on
55 different surface adsorption sites. In our lowest energy struc-
56 tures CO bind at both top and bridge sites, as supported by our
57 spectroelectrochemical experiments, which implies that the
58 quantity of CO molecules chosen for our DFT calculations is
59 feasible, taking into account the size of the unit cell.

In the lowest energy structure of GIOH on Pt(100) obtained
in our previous work¹¹, we revealed that GIOH binds with the
Pt(100) surface with the adsorption energy of -0.44 eV via the
O atom, where the distance between the O and Pt atom is
2.45 Å, and the angle between the bonds of the edge C atoms
and the surface normal is 79.46°. In the lowest-energy atomic
structure of GIOH on the Pt₆/Pt(100) surface, the GIOH mole-
cule favors binding on the triangle low coordinated Pt₆ edge
atom, whereas its total energy is 0.32–0.54 eV higher in the
terraces (see the configurations E – G in the Figure S10). The
lowest energy structure of GIOH on Pt₆/Pt(100) is modified by
comparison with GIOH on Pt(100)¹¹, i.e., the O-Pt bond
lengths are 2.32 Å and 2.21 Å, and the angles of between the
C-C bond and the normal to the surface are 78.55° and 90.39°
on the Pt(100) and Pt₆/Pt(100) surfaces, respectively, implying
stronger binding with the low coordinated Pt₆ atoms, which is
reflected in the adsorption energies, i.e. -0.45 eV and -0.79 eV,
respectively.

The structure of the mixture of 3CO and GIOH molecules on
Pt₆/Pt(100) (Figures 7 and S11) presents all of the molecules
located on the low coordination atoms Pt₆, in which GIOH
geometry is modified only slightly on the surface compared
with GIOH/Pt₆/Pt(100), i.e., binding to the edge Pt atom with
O-Pt bond length of 2.19 Å and C-C-normal angle of 89.45°.
Here, all of the CO molecules bind to the on-top sites of Pt₆, a
preference that can be explained by the intermolecular repul-
sion. Moving CO molecules to the terraces of Pt(100) increas-
es the total energy of the system (see B, C and D configura-
tions with their relative total energies of 0.07 eV, 0.22 eV, and
0.92 eV, respectively, in Figure S9). The adsorption energy for
3CO+GIOH/Pt₆/Pt(100) is slightly smaller (-7.07 eV) than if
we sum up the separate systems, i.e., (-6.43+0.79 = -7.22 eV),
which implies intermolecular interaction.

To obtain a better understanding of the binding mechanism
between the molecules and the defected Pt₆/Pt(100) surface,
we calculated the following properties of the systems: local
density of states, the changes in the substrate work function,
which reflects electron density rearrangement on the surfaces
upon the adsorption of molecules, and an effective charge of
every atom on the systems using Bader charge analysis. All
these properties are discussed in the Supporting Information
section.

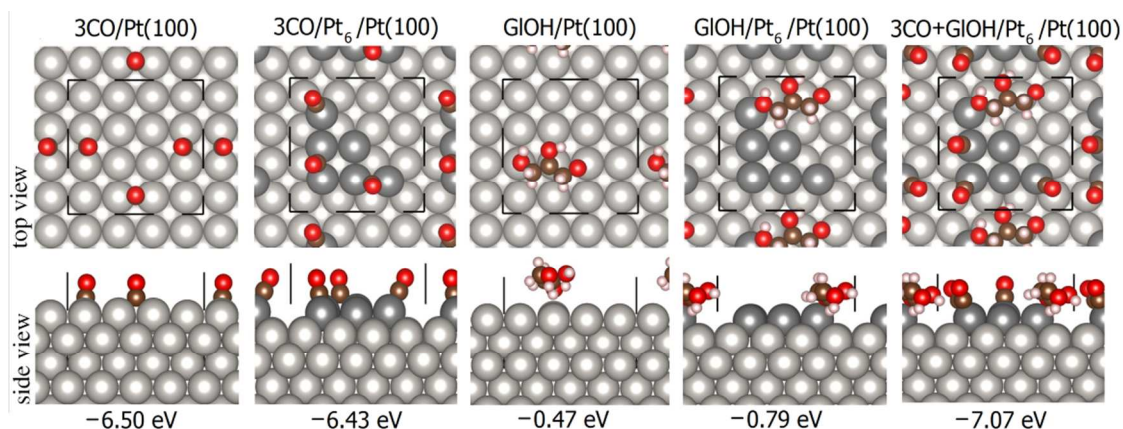


Figure 7. The lowest energy configurations for all of the systems and their adsorption energies.

DFT calculations, and electrochemical and spectroelectrochemical experiments.

We have shown in Figure 3 that the GEOR onset potential displaces towards positive potentials as the density of surface defects increases. We noted that this result does not agree with the fact that disturbed electrodes form Pt-OH species at lower potentials than Pt(100), which would permit Pt-OH and Pt-GIOH* (GIOH* = GIOH or GIOH residues) combination at lower potentials. On the other hand, the DFT calculations show that both CO and GIOH bind more strongly to the low coordinated Pt sites on the surface with defects. Therefore, the increase of the GEOR onset with increasing density of surface defects is probably because GIOH (and CO, which remains the only detected intermediate, although the presence of other species is probable, as noted during the discussion of Fig. 2) binds more strongly on these surfaces, indicating that the residues detachment is the rate determining step of the GEOR.

Interestingly, FTIR data showed that the presence of superficial defects on Pt favors GIOH C-C bond breaking, which seems to be connected (among other factors) with the surface ability to attach GIOH through at least two oxygen (or carbon) atoms. Correspondingly, DFT shows that GIOH attaches to a well ordered Pt(100) surface and to a disordered one at angles of approximately 21° and 10° , respectively, with respect to the surface. Most likely, the lower angle between the GIOH and the disturbed surface favors the molecule's attachment through multiple atoms, facilitating C-C bond breaking.

Figure 6 shows that on both surfaces, GIOH adsorption and oxidation occurs (or is detected) after the beginning of the on-top CO oxidation. The DFT results show that the CO-Pt bonds (on bridge and on-top positions) are much stronger than on-top GIOH-Pt for both surfaces, that is, in highly as well as in low coordinated Pt atoms. As a consequence, regardless of the exact nature of the early adsorbate, the generation of CO through the GIOH dissociative adsorption at low potentials does not permit detectable GIOH adsorption and further oxidation. In other words, the Pt-GIOH interaction is not strong enough to withdraw CO from the surface. This fact again suggests that the GEOR is mainly determined by the strength of the GIOH*-Pt bonds.

Finally, at high potentials (>0.80 V), where the GIOH molecule is easily oxidized, we showed that the C=O production is high on Pt100-0 and negligible on Pt0-100. Although more DFT calculations are needed, the computational simulations

showed that the GIOH-Pt bond strength is larger for the low coordination Pt atoms. Perhaps in this potential domain the GEOR to C=O is determined by the GIOH surface attachment rate, and this reaction step depends on the Pt-GIOH bond energy.

CONCLUSION

The generation of defects on Pt single crystals seems to be an interesting approach to studying the influence of defects on a given reaction. It is a new way of linking models with highly disturbed surfaces and could be used to determine the influence of defects in different chemical and electrochemical reactions.

The electrochemical behavior in acidic media of GIOH oxidation on Pt surfaces exhibits dependence on the surface order. The FTIR spectra elucidate this influence, revealing a potential dependence of the adsorbates coverage and products formed. The highly ordered surface Pt0-100 can oxidize GIOH at lower potentials than the highly disordered surface, Pt100-0.

DFT calculations show that both CO and GIOH bind more strongly to low coordinated Pt sites than when the surface is absent of defects. These results, together with electrochemical and spectroelectrochemical data, suggest that the Pt-CO bond breaking may be the GEOR rate determining step, primarily responsible for the relationship between GEOR onset and defect density.

ASSOCIATED CONTENT

AUTHOR INFORMATION

Corresponding Author

* email: pablo.fernandez@iqm.unicamp.br (P.S.F)

Present Addresses

* Chemistry Institute, State University of Campinas, PO Box 6154, 13083-970, Campinas SP, Brazil.

† Chemical Engineering Department, Federal University of São Carlos, P.O. Box 676, 13565-905, São Carlos - SP, Brazil.

ACKNOWLEDGMENT

Financial support from the Brazilian agencies: FAPESP (grants: 2014/01362-6, 2013/13749-0, 2013/21045-2, 2013/16930-7),

1
2
3
4
5
6
7
8
9
10
11
12
13
14
15
16
17
18
19
20
21
22
23
24
25
26
27
28
29
30
31
32
33
34
35
36
37
38
39
40
41
42
43
44
45
46
47
48
49
50
51
52
53
54
55
56
57
58
59
60

CNPQ (grants: 474590/2013-5, 454516/2014-2, 403142/2012-1, 484139/2013-4, 405695/2013-6, 305494/2012-0), CAPES (grants: PNP20131741-PNPD-USP/SC/QUÍMICA), FUNDCE (grant: 0091/12, process 23/200.583/2012).

Supporting Information.

Extra details of the electrochemical results. Details of the treatment of the FTIR and CVg data. Extra details and discussions about DFT calculations. This information is available free of charge via the Internet at <http://pubs.acs.org/>.

REFERENCES

- (1) Pagliaro, M.; Rossi, M. *The Future of Glycerol*, 2nd Edition. In *RSC Green Chemistry No. 8*; Royal Society of Chemistry, Cambridge, 2010.
- (2) Dasari, M.; Kiatsimkul, P.; Sutterlin, W.; Suppes, G. *App. Catal. A* **2005**, *281*, 225-231.
- (3) Chaminand, J.; Djakovitch, L.; Gallezot, P.; Marion, P.; Pinel, C.; Rosier, C. *Green Chem.* **2004**, *6*, 359-361.
- (4) Carretin, S.; McMorn, P.; Johnston, P.; Griffin, K.; Hutchings, G. *Chem. Commun.* **2002**, *7*, 696-697.
- (5) Katryniok, B.; Paul, S.; Belliere-Baca, V.; Rey, P.; Dumeignil, F. *Green Chem.* **2010**, *12*, 2079-2098.
- (6) Arechederra, R.; Treu, B.; Minteer, S. *J. Power Sources* **2007**, *173*, 156-161.
- (7) Kwon, Y.; Schouten, K.; Koper, M. *Chemcatchem* **2011**, *3*, 1176-1185.
- (8) Fernández, P.; Martins, M.; Martins, C.; Camara, G. *Electrochem. Commun.* **2012**, *15*, 14-17.
- (9) Coll, D.; Delbecq, F.; Aray, Y.; Sautet, P. *PCCP* **2011**, *13*, 1448-1456.
- (10) Liu, B.; Greeley, J. *J. Phys. Chem. C* **2011**, *115*, 19702-19709.
- (11) Tereshchuk, P.; Chaves, A. S.; Da Silva, J. L. F. *J. Phys. Chem. C* **2014**, *118*, 15251-15259.
- (12) Fernández, P. S.; Martins, C. A.; Angelucci, C. A.; Gomes, J. F.; Camara, G. A.; Martins, M. E.; Tremiliosi-Filho, G. *ChemElectroChem* **2015**, *2*, 263-268.
- (13) Gomes, J. F.; Tremiliosi-Filho, G. *Electrocatalysis* **2011**, *2*, 96-105.
- (14) Markovic, N. M.; Ross, P. N. *Surf. Sci. Rep.* **2002**, *45*, 121-229.
- (15) Lebedeva, N. P.; Koper, M. T. M.; Herrero, E.; Feliu, J. M.; van Santen, R. A. *J. Electroanal. Chem.* **2000**, *487*, 37-44.
- (16) Iwasita, T. *Electrochim. Acta* **2002**, *47*, 3663-3674.
- (17) Xia, X. H.; Liess, H. D.; Iwasita, T. *J. Electroanal. Chem.* **1997**, *437*, 233-240.
- (18) Orts, J. M.; Fernandezvega, A.; Feliu, J. M.; Aldaz, A.; Clavilier, J. *J. Electroanal. Chem.* **1990**, *290*, 119-133.
- (19) Sun, S. G.; Chen, A. C. *Electrochim. Acta* **1994**, *39*, 969-973.
- (20) Markovic, N. M.; Gasteiger, H. A.; Ross, P. N. *J. Phys. Chem.* **1995**, *99*, 3411-3415.
- (21) Dima, G. E.; Beltramo, G. L.; Koper, M. T. M. *Electrochim. Acta* **2005**, *50*, 4318-4326.
- (22) Souza-Garcia, J.; Ticianelli, E. A.; Climent, V.; Feliu, J. M. *Chem. Sci.* **2012**, *3*, 3063-3070.
- (23) Vidal-Iglesias, F. J.; Solla-Gullon, J.; Rodríguez, P.; Herrero, E.; Montiel, V.; Feliu, J. M.; Aldaz, A. *Electrochem. Commun.* **2004**, *6*, 1080-1084.
- (24) Tian, N.; Zhou, Z. Y.; Sun, S. G.; Ding, Y.; Wang, Z. L. *Science* **2007**, *316*, 732-735.
- (25) Welch, C. M.; Compton, R. G. *Anal. Bioanal. Chem.* **2006**, *384*, 601-619.
- (26) Clavilier, J.; Faure, R.; Guinet, G.; Durand, R. *J. Electroanal. Chem.* **1980**, *107*, 205-209.
- (27) Iwasita, T.; Nart, F. C. In *Advances in Electrochemical Science and Engineering Vol. 4*; Gerischer, H., Tobias, C. W., Eds.; Wiley-VCH Verlag GmbH: Weinheim, 1995.
- (28) Rodríguez, P.; Herrero, E.; Solla-Gullon, J.; Vidal-Iglesias, E. J.; Aldaz, A.; Feliu, J. M. *Electrochim. Acta* **2005**, *50*, 3111-3121.
- (29) Schnaidt, J.; Heinen, M.; Denot, D.; Jusys, Z.; Behm, R. *J. Electroanal. Chem.* **2011**, *661*, 250-264.
- (30) Perdew, J. P.; Burke, K.; Ernzerhof, M. *Phys. Rev. Lett.* **1996**, *77*, 3865-3868.
- (31) Kresse, G.; Hafner, J. *Phys. Rev. B* **1993**, *48*, 13115-13118.
- (32) Kresse, G.; Furthmuller, J. *Phys. Rev. B* **1996**, *54*, 11169-11186.
- (33) Blochl, P. E. *Phys. Rev. B* **1994**, *50*, 17953-17979.
- (34) Kresse, G.; Joubert, D. *Phys. Rev. B* **1999**, *59*, 1758-1775.
- (35) Vidal-Iglesias, F. J.; Solla-Gullon, J.; Campina, J. M.; Herrero, E.; Aldaz, A.; Feliu, J. M. *Electrochim. Acta* **2009**, *54*, 4459-4466.
- (36) Rodríguez, P.; Herrero, E.; Solla-Gullon, J.; Vidal-Iglesias, F. J.; Aldaz, A.; Feliu, J. M. *Electrochim. Acta* **2005**, *50*, 4308-4317.
- (37) Solla-Gullon, J.; Vidal-Iglesias, F. J.; Rodríguez, P.; Herrero, E.; Feliu, J. M.; Clavilier, J.; Aldaz, A. *Phys. Rev. B* **2004**, *108*, 13573-13575.
- (38) Souza-Garcia, J.; Angelucci, C. A.; Climent, V.; Feliu, J. M. *Electrochem. Commun.* **2013**, *34*, 291-294.
- (39) Domke, K.; Herrero, E.; Rodes, A.; Feliu, J. M. *J. Electroanal. Chem.* **2003**, *552*, 115-128.
- (40) Conway, B. *Prog. Surf. Sci.* **1995**, *49*, 331-452.
- (41) Gómez-Marin, A. M.; Clavilier, J.; Feliu, J. M. *J. Electroanal. Chem.* **2013**, *688*, 360-370.
- (42) Bjoerling, A.; Feliu, J. M. *J. Electroanal. Chem.* **2011**, *662*, 17-24.
- (43) Solla-Gullon, J.; Rodríguez, P.; Herrero, E.; Aldaz, A.; Feliu, J. M. *PCCP* **2008**, *10*, 1359-1373.
- (44) Al-Akl, A.; Attard, G.; Price, R.; Timothy, B. *PCCP* **2001**, *3*, 3261-3268.
- (45) Koper M. T. M. *Nanoscale* **2011**, *3*, 2054-2073.
- (46) Vidal-Iglesias, F. J.; Arán-Ais, R. M.; Solla-Gullon, J.; Rodríguez, P.; Herrero, E.; Feliu, J. *ACS Catal.* **2012**, *2*, 901-910.

1 SYNOPSIS TOC. Surfaces with a controlled density of defects with non-defined symmetries were electrochemically gener-
2 ated and characterized. Electrochemical and spectroelectrochemical experiments showed that the surfaces' catalytic perfor-
3 mance diminished as the density of defects increased.
4

